

Low-frequency noise in gallium nitride nanowire mechanical resonators

Jason M. Gray, Kris A. Bertness, Norman A. Sanford, and Charles T. Rogers

Citation: *Appl. Phys. Lett.* **101**, 233115 (2012); doi: 10.1063/1.4769445

View online: <http://dx.doi.org/10.1063/1.4769445>

View Table of Contents: <http://apl.aip.org/resource/1/APPLAB/v101/i23>

Published by the [American Institute of Physics](#).

Related Articles

Focused ion beam milling and deposition techniques in validation of mass change value and position determination method for micro and nanomechanical sensors

J. Appl. Phys. **112**, 114509 (2012)

Nanoscale spatial resolution probes for scanning thermal microscopy of solid state materials

J. Appl. Phys. **112**, 114317 (2012)

Size-variable droplet actuation by interdigitated electrowetting electrode

Appl. Phys. Lett. **101**, 234102 (2012)

Influence of a superficial field of residual stress on the propagation of surface waves—Applied to the estimation of the depth of the superficial stressed zone

Appl. Phys. Lett. **101**, 234104 (2012)

Influence of buoyancy-driven flow on mass transfer in a two-stream microfluidic channel: Introduction of cryoprotective agents into cell suspensions

Biomicrofluidics **6**, 044110 (2012)

Additional information on *Appl. Phys. Lett.*

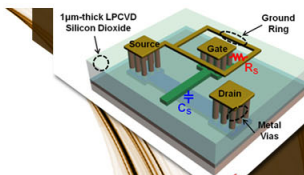
Journal Homepage: <http://apl.aip.org/>

Journal Information: http://apl.aip.org/about/about_the_journal

Top downloads: http://apl.aip.org/features/most_downloaded

Information for Authors: <http://apl.aip.org/authors>

ADVERTISEMENT



SURFACES AND INTERFACES

Focusing on physical, chemical, biological, structural, optical, magnetic and electrical properties of surfaces and interfaces, and more...

EXPLORE WHAT'S
NEW IN APL

SUBMIT YOUR PAPER NOW!



ENERGY CONVERSION AND STORAGE

Focusing on all aspects of static and dynamic energy conversion, energy storage, photovoltaics, solar fuels, batteries, capacitors, thermoelectrics, and more...

Low-frequency noise in gallium nitride nanowire mechanical resonators

Jason M. Gray,^{1,a)} Kris A. Bertness,² Norman A. Sanford,² and Charles T. Rogers¹

¹Department of Physics, University of Colorado, Boulder, Colorado 80309, USA

²National Institute of Standards and Technology, Boulder, Colorado 80305, USA

(Received 16 October 2012; accepted 16 November 2012; published online 7 December 2012)

We report on the low-frequency $1/f$ (flicker) parameter noise displayed by the resonance frequency of doubly clamped c-axis gallium nitride nanowire (NW) mechanical resonators. The resonators are electrostatically driven and their mechanical response is electronically detected via NW piezoresistance. With an applied dc voltage bias, a NW driven near its mechanical resonance generates a dc and Lorentzian rf current that both display $1/f$ noise. The rf current noise is proportional to the square of the derivative of the Lorentzian lineshape with a magnitude highly dependent on NW dc bias voltage conditions, consistent with a model wherein noise in the NW's electrical impedance leads to temperature noise from local Joule heating, which in turn generates resonance frequency noise via thermal expansion and the temperature-dependent Young's modulus. An example device with a 27.8 MHz resonance frequency experiences an approximate resonance frequency shift of -1.4 Hz/nW. The resonance frequency noise increases as the square of the bias voltage, indicating specific operating conditions that optimize the signal-to-noise ratio in proposed NW sensors. © 2012 American Institute of Physics. [<http://dx.doi.org/10.1063/1.4769445>]

Nanomechanical resonators offer exceptional performance for applications in mass,¹ force,² and displacement³ sensing. The resolution of such sensors for a given signal averaging time depends on multiple factors, including the transduction method, which determines the magnitude of measured signal for a given resonator deflection; the device geometry and material properties, including resonator mass and quality factor, Q ; and the noise performance of the system.⁴ Noise contributions include thermal displacement noise,⁵ measurement noise (e.g., from the readout amplifiers), and noise in the resonator's parameters (e.g., mechanical resonance frequency, f_0 , phase, or amplitude). Parameter noise in, for example, f_0 may be caused by adsorbing/desorbing of surface species,⁶ temperature fluctuations,⁵ and defect motion.⁷ In this paper, we report on the $1/f$ (flicker) parameter noise seen in the mechanical resonance frequency of gallium nitride (GaN) nanowire (NW) doubly clamped resonators sensed using a piezoresistive transduction scheme.

Piezoresistive nanomechanical resonator sensors transduce physical vibration into an electrical signal through strain-induced changes in electrical resistance. These sensors are attractive due to their scalability: resistance is relatively size-invariant, i.e., a NW resonator may be reduced in both length and diameter while maintaining the same resistance and piezoresistance. Thus, reducing the dimensions of the resonator, which is advantageous for sensing applications due to the lower mass and higher resonance frequency, does not reduce the efficacy of the piezoresistive transduction scheme.

The resonance frequency fluctuations observed in these piezoresistive resonators are consistent with a model wherein fluctuations in the resistance of the semiconducting NW lead to power and temperature fluctuations, correlated with fluctuations in NW mechanical resonance frequency. This model

is generally applicable to all systems utilizing piezoresistive transduction schemes and has important implications for the optimized operation of any resistive-based resonator sensor.

The resonators considered here are fabricated from c-axis oriented, single crystal GaN NWs. Briefly, the NWs are grown, catalyst free, via gas-source molecular-beam epitaxy on Si (111) substrates.⁸ The devices, as seen in Fig. 1(a), are fabricated on sapphire substrates using a combination of lithographic patterning and dielectrophoresis to freely suspend single NWs across $8\ \mu\text{m}$ – $10\ \mu\text{m}$ gaps, as described elsewhere.⁹ An applied rf voltage, V_{rf} , on the neighboring electrostatic gate induces NW vibration. A dc voltage difference, V_{dc} , applied between the ends of the NW results in both a dc current, I_{dc} , due to the NW resistance, and an rf current, I_{rf} , arising from the vibrating NW's time-dependent mechanical strain causing piezoresistive changes in NW resistance.⁹ We find that the piezoresistive gauge factor, α , defined by $\alpha = (\delta R/R)/\epsilon$, where $\delta R/R$ is the NW's relative resistance change and ϵ is its axial strain, for these GaN NWs is in the range of -10 to -30 , indicating that NW resistance decreases under tensile strain. The observed amplitude of I_{rf} is consistent with a piezoresistive effect rather than a piezoelectric field effect.¹⁰ I_{rf} is then amplified by a transimpedance amplifier and measured with an rf lock-in amplifier.

Figure 1(b) shows an example of I_{rf} upon sweeping the gate drive frequency through a NW's mechanical resonance. The Lorentzian mechanical response is transduced into a Lorentzian current response, here separated into components that are in phase ($I_{rf,in}$) and 90° out of phase ($I_{rf,out}$) with the applied V_{rf} gate drive signal. The left axis shows the current generated by vibration, while the right axis shows NW displacement as calibrated from the measured thermomechanical noise of the resonator.⁹ We have studied devices with values of f_0 ranging from 9 MHz to 36 MHz, set by NW diameter (typically 150 nm–250 nm) and lithographically selected length. Quality factors for these devices reach as

^{a)}Author to whom correspondence should be addressed. E-mail: jason.gray@colorado.edu. Telephone: 303-492-4659.

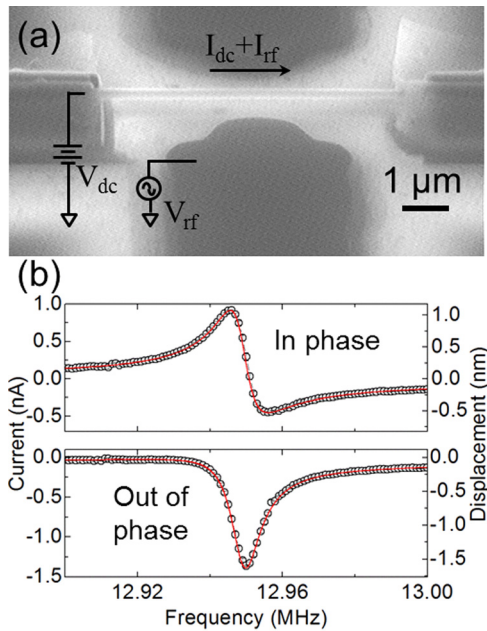


FIG. 1. (a) A scanning electron micrograph at 65° from normal of a doubly clamped, 160 nm diameter GaN NW resonator suspended over an 8 μm gap. Actuation is accomplished through a driving rf voltage V_{rf} applied to the electrostatic gate. Readout is accomplished through a dc voltage bias V_{dc} applied across the NW, inducing a dc current I_{dc} as well as an rf current I_{rf} on resonance due to the piezoresistive properties of GaN. (b) In-phase and out-of-phase components of I_{rf} due to sweeping the gate drive frequency through the NW's resonance, with $V_{dc} = 1.5$ V and $V_{rf} = 2$ V, taken at 10^{-4} Pa and 300 K. The figure displays a fitted Lorentzian resonator response (solid line), with the left axis showing $I_{rf,in/out}$ and the right axis showing the physical displacement of the resonator as calibrated from the measured thermal noise. Fitted parameters give $f_0 = 12.94898$ MHz \pm 40 Hz and $Q = 1320 \pm 10$.

high as 3000 under 10^{-4} Pa vacuum at room temperature, increasing to above 25 000 at 8 K.

Such devices can be used, for example, in mass or strain sensing applications by measuring a change δf_0 in f_0 .¹¹ In the case of a mass sensor, this change can be caused by, e.g., depositing additional mass on the resonator. To determine the accreted mass from a given δf_0 , we note that the resonance frequency goes as $2\pi f_0 = \sqrt{k_{eff}/M_{eff}}$, where k_{eff} is the effective resonator spring constant and M_{eff} is the effective vibratory mass. Assuming a small added mass δM such that $\delta M \ll M_{eff}$, it can be shown that

$$\delta M \approx -2 \frac{M_{eff}}{f_0} \delta f_0. \quad (1)$$

Thus, the minimum observable δM favors small resonator mass, large resonance frequencies, and is limited by the smallest measurable δf_0 , which, for these piezoresistively sensed resonators, is limited by the signal-to-noise performance of the I_{rf} measurement.⁴

To investigate the signal and noise behavior of I_{rf} , we operate NW resonators at various NW dc bias voltages, V_{dc} , electrostatic gate rf drive frequencies, f_g , and gate voltage amplitudes, V_{rf} . In the examples below, we limit V_{rf} to ensure a Lorentzian resonance line shape, i.e., a linear resonator response. The rf lock-in amplifier separates I_{rf} into the two phases of response, $I_{rf,in}$ and $I_{rf,out}$, and further, provides the time-dependence of these components within a 1 kHz bandwidth of the gate frequency, as set by the lock-in amplifier's time constant. We then independently analyze the power

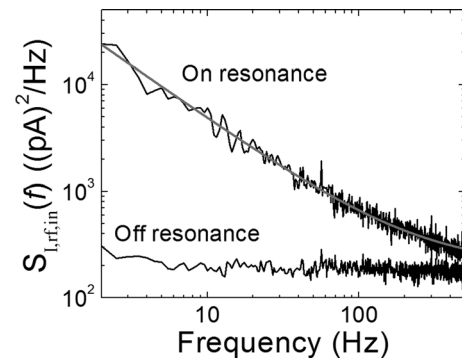


FIG. 2. Noise PSD of the component of I_{rf} in phase with the gate drive signal with $V_{dc} = 8$ V and $V_{rf} = 2$ V. When driven on resonance the noise predominantly shows a $1/f$ component. The gray line is a corresponding fit to amplifier white noise plus a $1/f$ contribution. Off resonance, only the white noise of the measurement electronics is seen.

spectral density (PSD) of each phase under various sensor operating conditions. We find that the electrical power dissipated in the NW, given by $P_{NW} = I_{dc} V_{dc}$, ignoring the small rf contribution, plays an important role in determining the noise performance of the sensor. For GaN NWs in the size range investigated here and for bias power $P_{NW} < \sim 5$ μW, the noise response at both phases is consistent with extrinsic transimpedance amplifier white noise of roughly 15 pA/ $\sqrt{\text{Hz}}$. However, for larger P_{NW} , a $1/f$ noise contribution can appear on either or both phases, with PSD amplitude dependent on P_{NW} and on gate drive frequency f_g . Figure 2 shows an example of the PSD of $I_{rf,in}$, $S_{I_{rf,in}}(f, f_g)$, where f refers to frequencies relative to f_g , from a 280 nm diameter, 8 μm long NW with $V_{dc} = 8$ V and $P_{NW} = 240$ μW. When the NW is driven on resonance at 27.53 MHz we see a substantial $1/f$ contribution, while with a drive frequency 100 kHz off resonance at 27.43 MHz we see only amplifier white noise.

The magnitude of the $1/f$ rf current noise, defined as $S_{I_{rf},in/out}(f = 1 \text{ Hz}, f_g)$ where the subscript *in/out* refers to either the in-phase or out-of-phase (quadrature) component of I_{rf} , displays a characteristic rf drive frequency and phase dependence as shown in Fig. 3, where again $P_{NW} = 240$ μW.

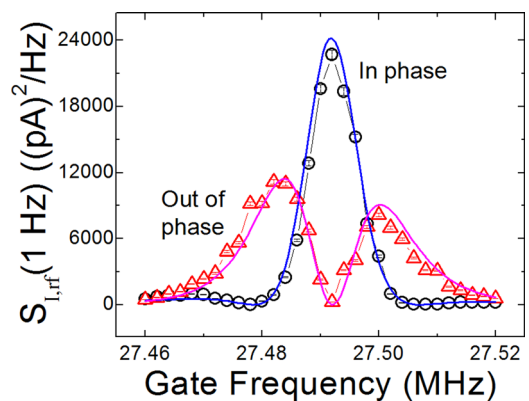


FIG. 3. Magnitude (at 1 Hz) of the $1/f$ noise PSD of the phase-sensitive NW rf current response, I_{rf} , as a function of gate drive frequency f_g , taken at 10^{-4} Pa, 300 K, $V_{dc} = 8$ V, and $V_{rf} = 2$ V for a NW with $f_0 = 27.491$ MHz. Circles are the noise magnitude for the in-phase signal, $I_{rf,in}$, triangles are the noise magnitude for the quadrature phase signal, $I_{rf,out}$. Solid lines, given by Eq. (2), are the predicted noise levels based on the observed $1/f$ noise in I_{dc} and the associated chain of power and resonance frequency derivatives. The structure is that of the square of the derivative of the Lorentzian response as determined by the fit to the resonance shape shown in Fig. 1(b).

The $1/f$ noise appears predominantly in the out-of-phase response when f_g is to either side of resonance, and predominantly in the in-phase signal on resonance. Comparing this result to Fig. 1(b), we note that these noise maxima correspond with local maxima in the magnitudes of the derivatives of the solid Lorentzian NW response curves. Thus, a possible explanation for the line shape of $S_{I_{rf},in/out}(1\text{ Hz}, f_g)$ is that noise in f_0 is generating a corresponding rf current noise δI_{rf} in the NW response, proportional to $\partial I_{rf,in/out}/\partial f_0$.

To test this hypothesis, we track f_0 and damping time ($=Q/\pi f_0$) by successively driving the NW into resonance, then removing the drive and extracting f_0 and damping time from the resulting free decay of I_{rf} . An example time record of such a free decay is seen in Fig. 4. In all cases, we find that the free decays are accurately fitted by a damped sinusoidal response. Fitted values for f_0 and damping time can be extracted roughly every 100 μs . Figure 5 shows an example of tracking f_0 for a NW resonator biased ($P_{NW} = 190\ \mu\text{W}$) to display significant $1/f$ noise in $S_{I_{rf},in}$ on resonance. Over the course of several minutes f_0 does indeed display a noisy variation, on the order of $\pm 2\text{ kHz}$ around 27.355 MHz. Furthermore, while tracking f_0 we simultaneously measure P_{NW} . Figure 5 shows that P_{NW} also displays a noisy variation, which is strongly anti-correlated with the f_0 variations. A parametric plot of f_0 versus P_{NW} demonstrates a linear relationship with $\partial f_0/\partial P_{NW} = -1.4 \pm 0.2\text{ Hz/nW}$. For the device examined in Fig. 3, direct measurement of $\partial f_0/\partial P_{NW}$ by shifting f_0 with dc power over the range $0.5\ \mu\text{W} \leq P_{NW} \leq 250\ \mu\text{W}$ results in $-1.38 \pm 0.02\text{ Hz/nW}$, in excellent agreement with the observed noise correlation.

PSD analysis shows that the spectra of f_0 and P_{NW} (S_{f_0} and $S_{P_{NW}}$, respectively) both display $1/f$ behavior. Further, the observed $S_{P_{NW}}$ is quantitatively the product of the bias voltage, V_{dc} , and the noise PSD of I_{dc} , $S_{I_{dc}}(f)$. The $1/f$ current noise is an order of magnitude higher than the noise in the dc voltage supply, and is therefore the controlling factor in determining NW power fluctuations. Such low-frequency power dissipation noise, caused, e.g., by noise in resistance,

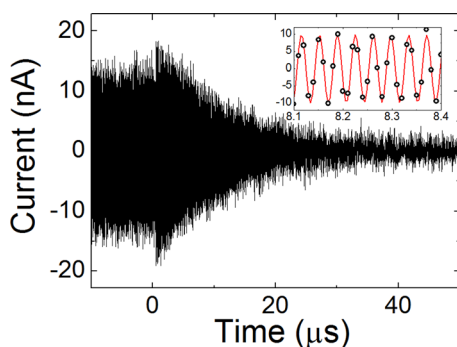


FIG. 4. A single-shot (no signal averaging) time record of NW current response under vibrational drive of $V_{rf} = 2\text{ V}$ at 27.444 MHz for $t < 0\ \mu\text{s}$, followed by free decay after setting $V_{rf} = 0\text{ V}$ at $t = 0\ \mu\text{s}$. The NW is dc biased at $240\ \mu\text{W}$ throughout the measurement. In the absence of drive, the NW is no longer constrained to oscillate at the drive frequency and resonates at its natural resonance frequency, f_0 , resulting in a temporary increase in vibrational amplitude at $t = 0\ \mu\text{s}$, and proceeds to decay exponentially. Inset: Sinusoidal oscillations within the exponentially decaying envelope. Fitting to the exponentially decaying sinusoidal response for $t > 0\ \mu\text{s}$ gives $f_0 = 27.4542 \pm 0.0001\text{ MHz}$ with a decay time τ of $12.8 \pm 0.1\ \mu\text{s}$, for a quality factor $Q = \pi f_0 \tau = 1100 \pm 10$.

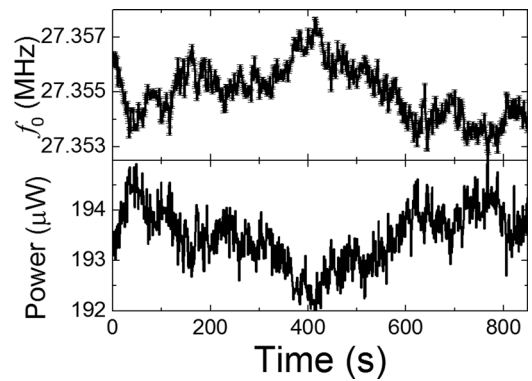


FIG. 5. Resonance frequency fluctuations showing a high degree of anti-correlation with the NW's power fluctuations, taken at 10^{-4} Pa , 300 K, $V_{dc} = 7\text{ V}$, and $V_{rf} = 2.8\text{ V}$. The power fluctuates due to fluctuating I_{dc} , likely due to NW dc impedance noise. Fluctuating power modifies the NW's temperature and results in a corresponding shift in resonance frequency. The correlation between f_0 and P_{NW} is $\partial f_0/\partial P_{NW} = -1.4 \pm 0.2\text{ Hz/nW}$.

is ubiquitous in semiconductor devices, including NWs¹⁰ and field effect transistors.¹²

Taken together, these observations suggest a model wherein noisy NW power dissipation leads to a noisy f_0 . This picture then explains the magnitude and structure of $S_{I_{rf},in/out}(f, f_g)$ by relating them to $S_{I_{dc}}(f)$ through power-induced changes in f_0 , given through the chain rule by

$$S_{I_{rf},in/out}(f, f_g) = \left(\frac{\partial I_{rf,in/out}}{\partial f_0} \right)^2 \left(\frac{\partial f_0}{\partial P_{NW}} \right)^2 \left(\frac{\partial P_{NW}}{\partial I_{dc}} \right)^2 S_{I_{dc}}(f), \quad (2)$$

where the partial derivatives are squared because the PSD measures mean-squared fluctuations per unit bandwidth. The first factor in Eq. (2) is determined by differentiating the Lorentzian fit seen in Fig. 1(b); the second factor is given by $\partial f_0/\partial P_{NW} = -1.38 \pm 0.02\text{ Hz/nW}$ as described above; and the third factor is the squared bias voltage, given that $P_{NW} = V_{dc} I_{dc}$. Note that Eq. (2) gives separate equations for the in-phase and out-of-phase components of I_{rf} , but both are related to the same $S_{I_{dc}}$. When multiplying these three derivatives with the measured $S_{I_{dc}}(1\text{ Hz})$, we arrive at the predicted $S_{I_{rf},in/out}(1\text{ Hz}, f_g)$ seen in the solid lines in Fig. 3. The agreement between the measured and predicted $S_{I_{rf},in/out}(1\text{ Hz}, f_g)$ strongly supports the hypothesis that the flicker noise in the mechanical resonance frequency is caused by fluctuations in f_0 resulting from fluctuations in NW power dissipation, largely due to NW resistance fluctuations.

The picture above explains the observed $1/f$ noise without requiring a detailed understanding of how fluctuations in P_{NW} lead to changes in resonance frequency. Here, we outline a simple picture based on NW heating to explain these fluctuations, and show it is in good agreement with observations. Within this picture, small changes δf_0 in the resonance frequency arise from small changes δP_{NW} in the power via the following chain rule:

$$\delta f_0 = \left(\frac{\partial f_0}{\partial \bar{T}} \right) \left(\frac{\partial \bar{T}}{\partial P_{NW}} \right) \delta P_{NW}, \quad (3)$$

where \bar{T} is the average NW temperature along its length. The relative shift in GaN NW cantilever mechanical resonance frequency with temperature is reported by Tanner

et al. as a decrease in frequency with increasing temperature of roughly $(1/f_0)(\partial f_0/\partial T) \approx -35$ parts per million (ppm) per K.¹³ The power fluctuations δP_{NW} are directly measured. We then estimate the GaN NW $\partial \bar{T}/\partial P_{NW}$ factor in Eq. (3) by solving a simple steady-state 1-dimensional heat equation with internal heat generation

$$\frac{\partial^2 T(x)}{\partial x^2} = -\frac{P_{NW}}{l^2 \cdot K_{th,NW}}, \quad (4)$$

where $K_{th,NW}$ is the thermal conductance in W/K (calculated through $K_{th,NW} = \kappa A/l$, where $\kappa = 1.3$ W/cm K is the thermal conductivity of GaN¹⁴ and A is the cross-sectional area) and l is the length of the GaN NW. The boundary conditions are given by $T|_{x=0} = T|_{x=L} = T_0 + P_{NW}/2K_{th,0}$, where T_0 is ambient temperature and $K_{th,0}$ is the thermal conductance of the interface between the metallic electrodes and the ends of the NW. Solving Eq. (4) gives the temperature profile along the NW as a linear function of dissipated power, and a quadratic function of position along the NW

$$T(x) = -\frac{P_{NW}}{2K_{th,NW}} \left(\frac{x^2}{l^2} - \frac{x}{l} \right) + T_0 + \frac{P_{NW}}{2K_{th,0}}. \quad (5)$$

The average NW temperature is given by $\bar{T} = 1/l \int_0^l T(x) dx = P_{NW}/12K_{th,NW} + T_0 + P_{NW}/2K_{th,0}$. Differentiating leads to $\partial \bar{T}/\partial P_{NW} = 1/12K_{th,NW} + 1/2K_{th,0}$. To determine a numerical value for $\partial \bar{T}/\partial P_{NW}$, we then require estimates for $K_{th,NW}$ and $K_{th,0}$.

For the device examined in Figs. 2 and 3, with dimensions of $r = 140$ nm and $l = 8$ μ m, we calculate $K_{th,NW} \approx 1$ μ W/K. To estimate the appropriate value for $K_{th,0}$, we use f_0 as a local thermometer, calibrated by measuring f_0 at a low enough bias power, $P_{NW} = 0.5$ μ W, that presumably NW temperature is nearly ambient, 300 K. Increasing P_{NW} to 240 μ W decreases f_0 by 314 kHz. With $f_0 = 27.8$ MHz and $(1/f_0)(\partial f_0/\partial T) \approx -35$ ppm/K, this frequency shift implies a temperature on the order of 320 K above ambient, i.e., 620 K. Substituting these values into the equation for \bar{T} above and solving for $K_{th,0}$ gives $K_{th,0} = 0.4$ μ W/K, a thermal conductance that is 40% of the estimated NW conductance and consistent with the 0.25 μ W/K NW-electrode thermal conductance estimated by Souidi, Dawson, and Gu.¹⁵ With the thermal conductances estimated, we calculate from above that $\partial \bar{T}/\partial P_{NW} \approx 1.3$ K/ μ W.

The predicted change in f_0 as a function of P_{NW} is then given by $\partial f_0/\partial P_{NW} = (\partial f_0/\partial T)(\partial \bar{T}/\partial P_{NW}) = (f_0)(-35 \times 10^{-6}/K)(1.3K/\mu W)$ with $f_0 = 27.8$ MHz, predicting a frequency shift of $\partial f_0/\partial P_{NW} = -1.3$ Hz/nW. As mentioned previously, the data in Fig. 5 indicate the true value is -1.4 ± 0.2 Hz/nW, displaying good agreement between the proposed heating theory and measurement.

Finally, we explore how the observed $1/f$ parameter noise affects the optimal operation of, e.g., a mass sensor. Considering only amplifier noise and not f_0 parameter noise, optimal resolution would be achieved by maximizing the amplitude of the signal—by operating at the largest possible drive force, and, in the case of piezoresistive readout of an ohmic NW, operating at the largest possible applied bias, V_{dc} , before reaching some system limit, such as severe NW

heating or extreme nonlinear response—to optimize the signal-to-noise ratio (SNR). In the presence of the observed f_0 parameter noise, however, Eq. (3) predicts that the rms f_0 noise in a given bandwidth will increase roughly as V_{dc}^2 , causing an overall reduction in the resolution of f_0 despite the increased signal at higher V_{dc} . Thus, there is an optimum operation point in NW bias voltage that balances amplifier noise with f_0 parameter noise, minimizing the resolvable δf_0 .

For the device described in Figures 2 and 3, this optimum point occurs at $V_{dc} = 3$ V, where total δf_0 (sum of flicker and white noise contributions in quadrature per root unit bandwidth) is 400 Hz/ $\sqrt{\text{Hz}}$. Below this V_{dc} , decreased signal compared to amplifier white noise raises δf_0 , e.g., to ~ 600 Hz/ $\sqrt{\text{Hz}}$ at 2 V, while above 3 V the increased $1/f$ noise in f_0 eventually dominates, e.g., $\delta f_0 \approx 2$ kHz/ $\sqrt{\text{Hz}}$ at 8 V. Returning to the mass sensor example discussed previously, we can use Eq. (1) to estimate the mass sensitivity of the device based on these uncertainties, where $M_{eff} \approx 1.9$ pg based on electron-micrograph-determined dimensions and f_0 is measured to be 27.8 MHz. This results in an optimum minimum detectable mass of $\delta M = 50$ ag/ $\sqrt{\text{Hz}}$ (1 ag = 10^{-18} g) at 3 V bias, increasing to 80 ag/ $\sqrt{\text{Hz}}$ and 270 ag/ $\sqrt{\text{Hz}}$ for 2 V and 8 V bias, respectively.

This 3 V optimum bias point is appropriate for the particular amplifier used here, whose 15 pA/ $\sqrt{\text{Hz}}$ current noise is equivalent to an effective displacement noise of 130 pm/ $\sqrt{\text{Hz}}$ for the ~ 8.7 pm/pA piezoresistive transduction gain at this bias. For comparison, the thermomechanical displacement noise⁹ for this NW, on resonance, is approximately 0.05 pm/ $\sqrt{\text{Hz}}$. With a lower-noise amplifier—such as a near-quantum limited Josephson parametric amplifier¹⁶—whose noise is thermomechanically limited, the optimum bias point under similar drive conditions would drop to approximately 0.08 V, with corresponding δf_0 and δM of 0.2 Hz/ $\sqrt{\text{Hz}}$ and 30 zg/ $\sqrt{\text{Hz}}$ (1 zg = 10^{-21} g), respectively.

In summary, we have investigated low-frequency noise in doubly clamped GaN NW resonators. At low bias voltage across the NW, the system noise consists of the white noise of the readout electronics. At higher bias voltage, flicker noise from power-induced frequency fluctuations becomes the dominant noise term. A simple thermal model is in strong agreement with observations, suggesting that fluctuations in NW electrical transport lead to fluctuations in mechanical resonance frequency. These results are generally applicable to any piezoresistive resonator, and so for sensing applications it becomes critically important to operate at the optimum bias power that balances maximizing the SNR with minimizing thermal parameter noise.

The studies conducted by the authors from the University of Colorado-Boulder are supported by the DARPA Center on Nanoscale Science and Technology for Integrated Micro/Nano-Electromechanical Transducers (iMINT), supported by the Defense Advanced Research Projects Agency (DARPA) N/MEMS S&T Fundamentals program under Grant No. N66001-10-1-4007 issued by the Space and Naval Warfare Systems Center Pacific (SPAWAR). We also acknowledge early funding support from the National Science Foundation (NSF-CMMI).

- ¹Y. T. Yang, C. Callegari, X. L. Feng, K. L. Ekinci, and M. L. Roukes, *Nano Lett.* **6**, 583 (2006).
- ²H. J. Mamin and D. Rugar, *Appl. Phys. Lett.* **79**, 3358 (2001).
- ³J. B. Hertzberg, T. Rocheleau, T. Ndukum, M. Savva, A. A. Clerk, and K. C. Schwab, *Nat. Phys.* **6**, 213 (2010).
- ⁴K. L. Ekinci, Y. T. Yang, and M. L. Roukes, *J. Appl. Phys.* **95**, 2682 (2004).
- ⁵A. N. Cleland and M. L. Roukes, *J. Appl. Phys.* **92**, 2758 (2002).
- ⁶J. Vig and Y. Kim, *IEEE Trans. Ultrason. Ferroelectr. Freq. Control* **46**, 1558 (1999).
- ⁷A. Nowick and B. Berry, *Anelastic Relaxation in Crystalline Solids* (Academic, New York, 1972).
- ⁸K. A. Bertness, A. Roshko, L. M. Mansfield, T. E. Harvey, and N. A. Sanford, *J. Cryst. Growth* **310**, 3154 (2008).
- ⁹J. M. Gray, C. T. Rogers, K. A. Bertness, and N. A. Sanford, *J. Vac. Sci. Technol. B* **29**, 052001 (2011).
- ¹⁰X. Wang, J. Zhou, J. Song, J. Liu, N. Xu, and Z. L. Wang, *Nano Lett.* **6**, 2768 (2006).
- ¹¹T. R. Albrecht, P. Grutter, D. Home, and D. Rugar, *J. Appl. Phys.* **69**, 668 (1991).
- ¹²K. S. Ralls, W. J. Skocpol, L. D. Jackel, R. E. Howard, L. A. Fetter, R. W. Epworth, and D. M. Tennant, *Phys. Rev. Lett.* **52**, 228 (1984).
- ¹³S. M. Tanner, J. M. Gray, C. T. Rogers, K. A. Bertness, and N. A. Sanford, *Appl. Phys. Lett.* **91**, 203117 (2007).
- ¹⁴E. K. Sichel and J. I. Pankove, *J. Phys. Chem. Solids* **38**, 330 (1977).
- ¹⁵A. Soudi, R. D. Dawson, and Y. Gu, *ACS Nano* **5**, 255 (2011).
- ¹⁶J. D. Teufel, T. Donner, D. Li, J. W. Harlow, M. S. Allman, K. Cicak, A. J. Sirois, J. D. Whittaker, K. W. Lehnert, and R. W. Simmonds, *Nature* **475**, 359 (2011).